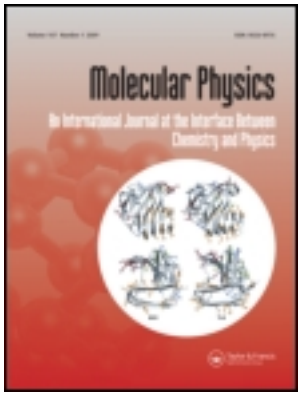

Molecular Physics: An International Journal at the Interface Between Chemistry and Physics
Publication details, including instructions for authors and subscription information:
http://www.tandfonline.com/loi/tmph20

Structure and dynamics of the high gerade Rydberg states of D_2 in the vicinity of the adiabatic ionization threshold

TH. A. Paul [a], H. A. Cruse [a], H. J. Wörner [a] & F. Merkt [a]
[a] Laboratorium für Physikalische Chemie, ETH Zurich, Wolfgang Pauli Str. 10, 8093, Zurich, Switzerland
Published online: 16 May 2007.

To cite this article: TH. A. Paul, H. A. Cruse, H. J. Wörner & F. Merkt (2007) Structure and dynamics of the high gerade Rydberg states of D_2 in the vicinity of the adiabatic ionization threshold, Molecular Physics: An International Journal at the Interface Between Chemistry and Physics, 105:5-7, 871-883, DOI: 10.1080/00268970601146898

To link to this article: http://dx.doi.org/10.1080/00268970601146898

Molecular Physics, Vol. 105, Nos. 5–7, 10 March–10 April 2007, 871–883

Taylor & Francis
Taylor & Francis Group

Structure and dynamics of the high gerade Rydberg states of D_2 in the vicinity of the adiabatic ionization threshold†

TH. A. PAUL, H. A. CRUSE, H. J. WÖRNER and F. MERKT*
Laboratorium für Physikalische Chemie, ETH Zurich, Wolfgang Pauli Str. 10, 8093 Zurich, Switzerland

(*Received 7 November 2006; in final form 30 November 2006*)

The structure and dynamics of the gerade Rydberg states of para D_2 in the vicinity of the $X^+2\Sigma_g^+$ ($v^+ = 0$) ionization threshold have been studied by resonance-enhanced two-photon excitation spectroscopy via selected rotational levels of the $B\,^1\Sigma_u^+$ ($v = 2$ and 3) states. The autoionization and predissociation dynamics were investigated by monitoring the D_2^+ and $D(n = 2)$ fragments, and long-lived Rydberg states were identified by measuring the delayed pulsed field ionization signal. The spectra, which consist of extended Rydberg series converging on the first rotational levels of the D_2^+ ion, reveal strong perturbations near the positions of low-n ($n = 4$–9) Rydberg states belonging to series converging on vibrationally excited levels of the cation and of Rydberg states of intermediate n values ($n = 23$–26) belonging to series converging on rotationally excited levels of D_2^+. The predissociation of the high-n Rydberg states below the $v^+ = 0, N^+ = 1$ ground state of para D_2^+ is mediated by the interaction with predissociative low-n, $v^+ \geq 1$ Rydberg states and is strongly influenced by vibrational and rotational channel interactions. The channel interactions are subject to restrictive selection rules and numerous Rydberg states appear metastable on the experimental time scale of 3 μs. A map of these long-lived Rydberg states has been established. Analysis of the Rydberg series by multichannel quantum defect theory led to the determination of effective quantum defect parameters for the channels associated with the ground vibrational level of D_2^+ and of an improved value for the ionization energy of the B ($v = 2, J = 0$) state.

Keywords: Rydberg states; Photoionization; Predissociation; Molecular hydrogen; Autoionization

1. Introduction

The Rydberg spectrum of H_2 represents a prototypical system for the study of the interaction between an electron and a molecular cation. In the vicinity of the lowest ionization thresholds, this interaction leads to rich dynamics: autoionization and predissociation compete and strongly depend on the Rydberg electron principle and orbital angular momentum quantum numbers n and ℓ and on the vibrational (v^+) and rotational (N^+) quantum numbers of the H_2^+ ion core [1–15].

The singlet gerade Rydberg states of H_2 show particularly complex behaviour because they interact with the $(2p\sigma_u)^2\,^1\Sigma_g^+$ doubly excited state. At low n values, this interaction leads to electronic states with a double-well potential such as the EF and the GK states [8, 16]. At high n values, the interaction causes the predissociation of gerade Rydberg levels associated with a vibrationally excited ion core [8, 9]. The $v^+ = 0$ Rydberg states, however, are largely immune to predissociation because the vibrational wave function does not extend to sufficiently large internuclear distances. Predissociation in these states is mediated by vibrational channel interactions with predissociative low-n Rydberg states associated with vibrationally excited H_2^+. These low-n Rydberg states are responsible for the very irregular appearance of the Rydberg spectrum of H_2 and for the seemingly random variation with n of the lifetimes and decay mechanisms of the $v^+ = 0$ Rydberg levels. They are commonly referred to as 'interlopers'.

Rottke and Welge [9] have developed a method to obtain a global view of the dynamics of the gerade

†This article is dedicated to Professor John M. Brown on the occasion of his 65th Birthday.

*Corresponding author. Email: merkt@xuv.phys.chem.ethz.ch

Molecular Physics
ISSN 0026–8976 print/ISSN 1362–3028 online © 2007 Taylor & Francis
http://www.tandf.co.uk/journals
DOI: 10.1080/00268970601146898

Rydberg states of H_2 based on a resonant two-photon excitation scheme via selected rovibrational levels of the $B\,^1\Sigma_u^+$ state and the simultaneous detection of the ionization and dissociation products. Their investigations of H_2 also revealed the existence of long-lived, low-ℓ Rydberg levels close to the ionization threshold. Their method has been adopted by Glab and coworkers, who recorded spectra of the s and d Rydberg states of H_2 in the vicinity of the first ionization threshold at higher spectral resolution ($\approx 0.2\,\mathrm{cm}^{-1}$) [13]. Later studies have focused on very high resolution measurements of millimeter wave transitions from selected long-lived high-n s and d Rydberg levels to neighbouring p and f Rydberg levels, which provided information on the hyperfine structure of the high-n Rydberg states and of the ion core levels of ortho H_2 [15, 17].

Experimental progress in studies of the Rydberg spectrum of H_2 has been accompanied, and stimulated, by theoretical investigations using multichannel quantum defect theory (MQDT) [1, 2, 4, 8, 10–12, 15, 18]. At present, MQDT is able to reproduce experimental data on the ungerade Rydberg states almost perfectly, including their hyperfine structure [15]. Considerable progress has also been made in the treatment of the structure and dynamics of the gerade (s and d) Rydberg states [8, 10–12, 19], the treatment of which, however, remains a theoretical challenge for the reasons outlined above.

The situation is less satisfactory for the Rydberg states of the isotopomers HD and D_2 for which less experimental data and very few theoretical studies are available. Information on the ungerade Rydberg states of HD has been obtained by single-photon excitation from the ground state [20–22] and selected regions of these spectra have been analysed by MQDT [22, 23]. The autoionization and predissociation dynamics of the gerade Rydberg states of HD in the vicinity of the first ionization threshold have been studied experimentally [24] but no MQDT analysis of the gerade Rydberg states of HD has been reported to date.

Several theoretical and experimental investigations, primarily of low-n Rydberg states of D_2, have been reported [25–33] and the extensive set of spectroscopic data acquired in the laboratory of Dieke has been summarized and analysed in [34]. Hardly any information is currently available on the high-n gerade Rydberg states of D_2 in the vicinity of the $v^+ = 0$ ionization threshold.

Several years ago, we started systematic investigations of the Rydberg states of molecular hydrogen by high-resolution laser and millimeter wave spectroscopy [15, 17]. The aim of these investigations is to obtain a complete description of the structural and dynamical properties of highly excited electronic states of molecular hydrogen which includes the effects of the electron and nuclear spins. They are carried out in two steps: single- and multiphoton laser excitation are first used in combination with pulsed electric field ionization to obtain, at a spectral resolution in the range 0.1–1 GHz, a global survey of the rovibrational structure of the Rydberg states and to establish maps of the predissociative, the autoionizing and the long-lived Rydberg levels [15, 22]. Millimeter wave spectra of Rydberg–Rydberg transitions are then recorded from each long-lived state at sub-MHz resolution to fully resolve the fine and hyperfine structures [15, 17].

We describe here the results of an investigation of the gerade Rydberg states of para D_2 by high-resolution laser spectroscopy and provide a global view of their structure and dynamics near the lowest ionization threshold and a map of all long-lived s and d Rydberg states in this region. The results of our investigation of the hyperfine structure of the long-lived Rydberg states of para D_2 will be reported separately [35].

The smaller vibrational and rotational constants of D_2^+ compared with H_2^+ imply a much higher density of low-n predissociative interlopers in the vicinity of the $v^+ = 0$ ionization threshold, resulting in more complex spectral structures and, potentially, faster decay dynamics. It was therefore not clear, at the outset of the present study, whether long-lived s and d Rydberg states of D_2 would be observed at all.

The present investigation of the lifetimes and decay dynamics in Rydberg states of molecular hydrogen is also relevant in the context of recent attempts to control the translational motion of molecular hydrogen excited to long-lived Rydberg states using inhomogeneous electric fields [36–38]. The region below the first ionization limit ($X\,^2\Sigma_g^+$ ($v^+ = 0$, $N^+ = 1$) in para D_2) is particularly important for these experiments because autoionization is not possible energetically and a rapid decay that would prohibit an efficient control of the translational motion can only be caused by predissociation. This region is the primary focus of the present article.

2. Experimental procedure

A schematic energy level diagram illustrating the resonant $(1 + 1')$ two-photon excitation scheme employed for accessing the high-n, low-l gerade Rydberg states of para D_2 in the vicinity of the X^+ ($v^+ = 0$, $N^+ = 1$ and 3) ionization thresholds is illustrated in figure 1. The $v' = 2$ and 3 levels of the B state were chosen as intermediate levels in this excitation scheme because the $B\,^1\Sigma_u^+$ ($v = 2, 3$) $\leftarrow X\,^1\Sigma_g^+$ ($v = 0$)

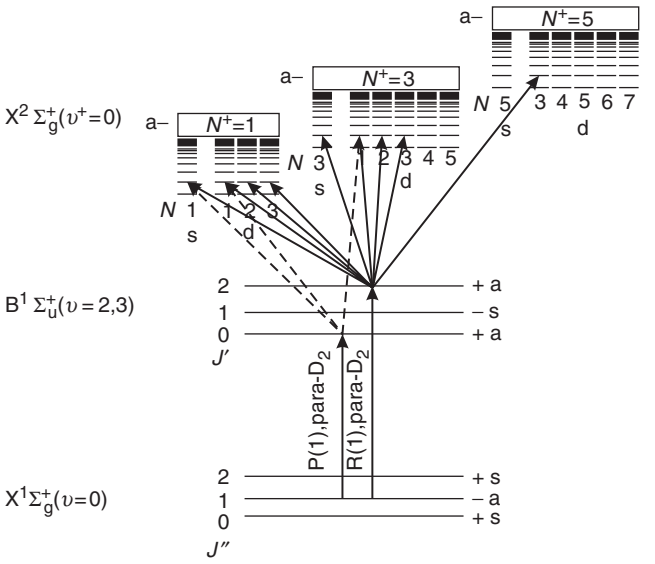

Figure 1. Schematic energy level diagram illustrating the resonant $(1+1')$ two-photon excitation scheme employed for accessing the high-n, low-l gerade Rydberg states of para D_2 in the vicinity of the X^+ ($v^+=0$, $N^+=1$ and 3) ionization thresholds.

transitions are characterized by large Franck–Condon factors and lie in a range where VUV radiation can easily be generated.

At sufficiently high n values, the s and d Rydberg states of D_2 can be labelled using Hund's case (d) nomenclature as $n\ell N_N^+$, where n represents the principal quantum number, ℓ the orbital angular momentum quantum number of the Rydberg electron, N^+ the ion core rotational angular momentum quantum number and N the quantum number associated with the total angular momentum without spins. The allowed transitions from the intermediate $B\,^1\Sigma_u^+$ state, which is the lowest member of the p Rydberg series, can be derived using the electric dipole selection rules $\Delta J=0,\pm1$, $u \leftrightarrow g$, $a \nleftrightarrow s$, $+ \leftrightarrow -$, where a/s represent the nuclear spin symmetry (a for para D_2) and $+/-$ the parity of the rovibronic states. Nine series, indicated by full lines in figure 1, are accessible using the B–X R(1) transition (i.e. $s1_1$, $d1_1$, $d1_2$, $d1_3$, $s3_3$, $d3_1$, $d3_2$, $d3_3$, $d5_3$) and three series, indicated by dashed lines in figure 1, using the B–X P(1) transition (i.e. $s1_1$, $d1_1$, $d3_1$).

The vacuum ultraviolet (VUV) radiation required to drive the B–X(2, 3–0) transitions was generated by two-photon resonance-enhanced sum-frequency mixing ($\tilde{\nu}_{VUV}=2\tilde{\nu}_1+\tilde{\nu}_2$) in xenon using two tunable lasers. The wave number $\tilde{\nu}_1$ of the first laser was kept fixed at the position of the $5p^5 6p[1/2]_0 \leftarrow 5p^6\,{}^1S_0$ two-photon resonance of Xe at $2\tilde{\nu}_1 \approx 80\,119\,cm^{-1}$ and the wave number $\tilde{\nu}_2$ of the second laser was adjusted so that the VUV wave number corresponded to the R(1) or P(1) lines of the B ($v=2,3$)–X ($v=0$) transitions.

Both laser beams were overlapped spatially and focused into a four-wave mixing chamber (background pressure 10^{-8} mbar) to a common point located immediately below the orifice of a pulsed nozzle releasing pulses of xenon gas (purity 4.0, PanGas) at the 25 Hz repetition rate of the lasers. The sum-frequency radiation was separated from the fundamental beams and from radiation generated by other nonlinear processes using a vacuum monochromator equipped with a platinum-coated diffraction grating. The toroidal geometry of the grating permitted recollimation of the diverging VUV beam. The selected VUV radiation entered the photoexcitation chamber via a pinhole and intersected a skimmed supersonic expansion of D_2 (99.8% purity, PanGas) at right angles.

The UV radiation in the range 32 000–35 000 cm^{-1} required to induce transitions from the B ($v=2$ and 3) intermediate levels to high Rydberg states located in the vicinity of the X^+ ($v^+=0$) ionization threshold was generated by doubling the frequency of a dye laser in a β barium borate (BBO) crystal. This laser beam was introduced into the photoexcitation region through a quartz window and intersected the VUV laser and D_2 gas beams at right angles in the middle of a set of resistively coupled extraction plates. This set of plates and the adjacent field-free flight tube were surrounded by a double layer of mumetal magnetic shielding and formed a linear time-of-flight (TOF) mass spectrometer. The relative polarizations of the UV and VUV beams were parallel [perpendicular] for the spectra recorded via the B ($v=2$) [B ($v=3$)] intermediate level.

Transitions from the selected intermediate rovibrational levels of the B state of D_2 to Rydberg states were recorded by monitoring the D_2^+ ions produced either by autoionization or by the delayed pulsed field ionization of Rydberg states as a function of the wave number of the UV laser. The gerade Rydberg states of D_2 belonging to series converging to vibrationally excited levels of D_2^+ are predissociative and form D ($n=2$) atomic fragments. If predissociation occurs within the duration of the UV laser pulse, i.e. within 5–10 ns, then the D ($n=2$) fragments can be ionized by the UV radiation and a D^+ signal detected [9, 24, 39]. However, the detection scheme is not sensitive to Rydberg states which predissociate to form two ground state D atoms, nor to Rydberg states which predissociate after the UV laser pulse has ended. The D^+ and D_2^+ ions were extracted by a delayed pulsed electric field towards a microchannel plate detector. Setting temporal gates on the ion TOF spectrum at the positions corresponding to the flight times of the D^+ and D_2^+ ions enabled the simultaneous recording of predissociation and

ionization spectra. Moreover, monitoring the D_2^+ signal as a function of the delay between the laser pulses and the pulsed electric field permitted us to obtain information on the lifetimes of the Rydberg levels.

Two different laser systems have been used in the course of this research. To obtain an overall picture of the structure and dynamics of the Rydberg states of D_2 in the region of the first ionization thresholds, survey scans were recorded at low resolution ($0.2\,cm^{-1}$) using VUV and UV radiation generated from the output of commercial pulsed dye lasers (Lambda Physik, Scanmate) [40]. High-resolution spectra were recorded using home-built lasers producing near-Fourier-transform-limited pulses of VUV and UV radiation. The VUV radiation, with a bandwidth of 55 MHz, was generated by amplifying the single-mode output of a titanium sapphire (Ti:Sa) ring laser in Nd:YAG-pumped Ti:Sa crystals in a system designed for the generation of pulses of adjustable shape and duration using acousto-optic modulators [41, 42]. The UV radiation with a bandwidth of 100 MHz was produced by doubling the pulse-amplified output of a ring dye laser system as described in [43]. The high-resolution spectra were used to study the fine structure of the high Rydberg states, to obtain information on their lifetimes, to derive precise and accurate wave numbers for the transitions from the B ($v=2$) intermediate level to the high Rydberg states and, by extrapolation of the Rydberg series, also to the D_2^+ ionic levels.

The absolute frequency of the dye ring laser was calibrated by guiding a reference beam through an I_2 cell at room temperature, recording the laser-induced-fluorescence spectrum and comparing the measured wave numbers with those listed in published calibration tables [44, 45]. Two Vernier étalon transmission signals were recorded simultaneously with the D_2 spectra and permitted the linearization of individual 10 GHz scan segments to an accuracy of 80 MHz in the UV. Connecting adjacent scan segments using the electronic version of the iodine atlas for calibration [46] yielded a residual relative uncertainty of 30 MHz. The relative line positions in the spectra could be determined with an uncertainty of ≈ 160 MHz, which corresponds to twice the frequency step size chosen when scanning the visible ring laser output. In addition to these three sources of uncertainties in the relative transition wave numbers, uncertainties in the absolute wave numbers also had to be considered arising from chirp, pressure and Stark shifts, which were estimated as described in [47], Doppler shifts, and from the absolute frequency uncertainty in the I_2 reference transitions.

To determine the Doppler shift resulting from a possible deviation α of the angle between the UV laser and the D_2 gas beam from 90°, spectra of individual sharp transitions (e.g. to the $40d1_1$ Rydberg state) were recorded using first neat D_2 (beam velocity $v^{D_2} = 2060(200)\,m\,s^{-1}$) and then a 1:10 D_2:Kr gas mixture (beam velocity $v^{D_2/Kr} = 380(40)\,m\,s^{-1}$). The Doppler shift, $\Delta\nu^{D_2}$, could then be obtained using

$$\Delta\nu^{D_2} = \nu_{exp}^{D_2} \cdot \frac{\nu^{D_2/Kr} - \nu^{D_2}}{\nu_{exp}^{D_2} - \nu_{exp}^{D_2/Kr}}, \qquad (1)$$

with $\nu^{D_2/Kr}$ and ν^{D_2} representing the measured transition frequencies for D_2 seeded in krypton and neat D_2, respectively. Uncertainties in the line centres and a conservative 10% uncertainty in the assumed beam velocities were propagated through the calculation, contributing an uncertainty of 290 MHz in the determination of the transition frequencies.

The error budget of the present measurements of transition frequencies from the B($v=2$) level of D_2 to high Rydberg states located in the vicinity of the lowest ionization threshold is summarized in table 1. The uncertainty in the Doppler shift dominates the total absolute uncertainty of 330 MHz.

3. Experimental results

The main experimental results are presented in figures 2 and 3 and consist of survey spectra recorded at a resolution of $0.2\,cm^{-1}$ in the vicinity of the adiabatic ionization threshold of D_2 in the range 124 600–125 000 cm^{-1} (figure 2) and high-resolution spectra of the region of the high Rydberg states just below the $v^+=0$, $N^+=1$ ionization threshold (figure 3). In these figures and in the rest of the article, we use the notation $n\ell N_N^+$ to designate the Rydberg levels converging on rotational levels of the $v^+=0$ ionic state and the notation $n\ell N_N^+(v^+)$ to label the Rydberg states converging on vibrationally excited core levels. The positions of all transitions are listed in appendix [48].

3.1. *Overview of the region around the $v^+=0$, $N^+=1$ and $N^+=3$ ionization thresholds and assignment of vibrational interlopers*

Overview spectra of the region around the $X\,^2\Sigma_g^+$ $v^+=0$, $N^+=1$ and $N^+=3$ thresholds of D_2 recorded using the lower-resolution dye-laser system are displayed in figure 2. The upper and lower pairs of spectra were obtained with the first laser fixed on the R(1) and P(1) transitions to the $B\,^1\Sigma_u^+$ ($v=3$) state, respectively. Panels (a) and (c) represent the ion signal recorded in the D_2^+ mass channel, whereas panels (b) and (d) display the D^+ ion signal. As explained in section 2, the D^+ signal results from D_2 Rydberg states which predissociate to

Table 1. Relative and absolute uncertainties in the measurement of the wave numbers of the $n\ell N_N^+(v^+) \leftarrow B\ ^1\Sigma_g^+\ (v = 2, J = 0, 2)$ transitions.

	Source of uncertainty	Uncertainty in UV (MHz)
Sources of uncertainties in the relative line positions	Location of maximum of line profile	160
	Scan linearization	80
	Relative I_2 calibration	30
Total relative uncertainty		**180**
Sources of systematic errors potentially affecting the absolute line positions	Doppler shift	290
	Chirp shift	60
	Stark shift	< 60
	Pressure shift	< 60
	I_2 calibration	120
Total absolute uncertainty		**330**

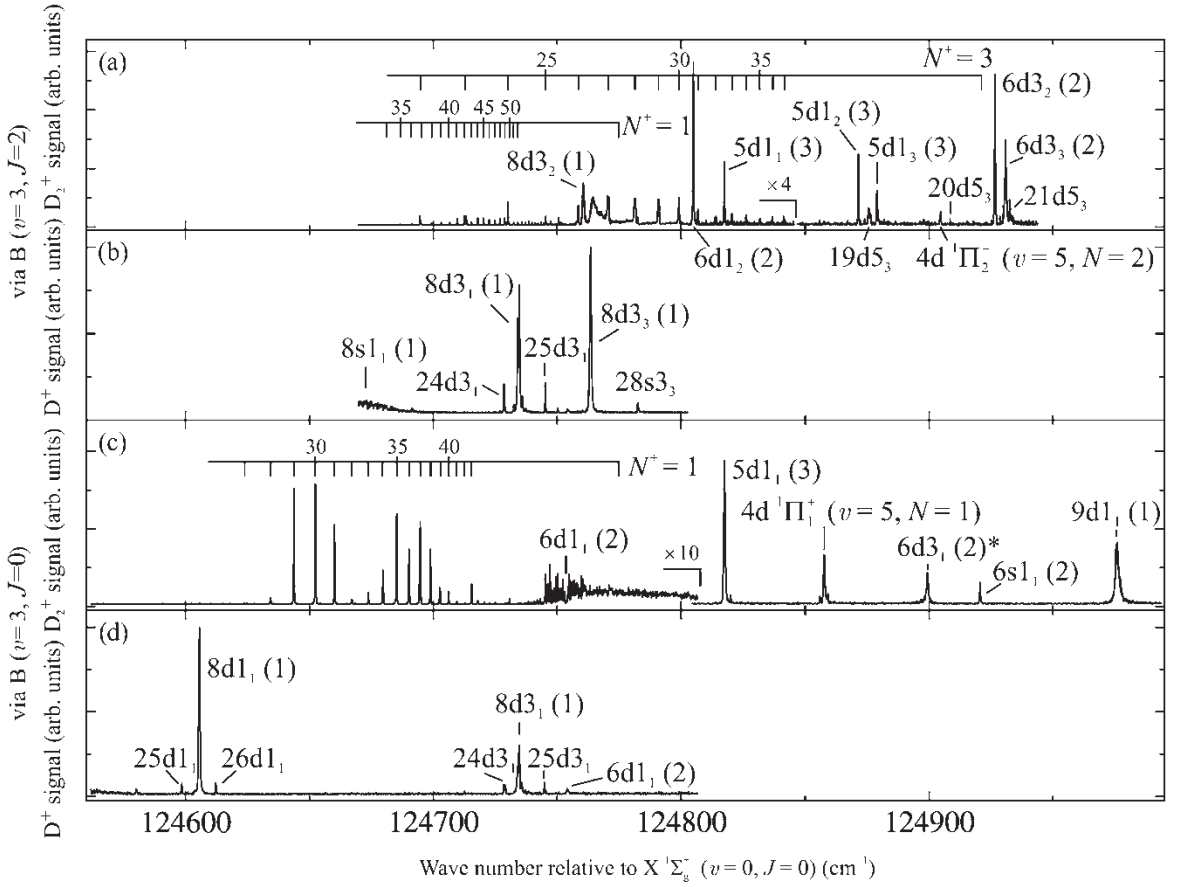

Figure 2. Overview spectra of the region around the $X\,^2\Sigma_g^+$ ($v^+ = 0$, $N^+ = 1$ and $N^+ = 3$) ionization thresholds of D_2 recorded using the lower-resolution dye-laser system. The upper and lower pairs of spectra were obtained with the first laser fixed on the R(1) and P(1) transitions to the $B\,^1\Sigma_u^+$ ($v = 3$) state, respectively. Traces (a) and (c) represent the ion signal recorded in the D_2^+ mass channel, whereas traces (b) and (d) display the D^+ ion signal. The wave number scale is relative to the position of the $X\,^1\Sigma_g^+(v = 0, J = 0)$ ground neutral state of D_2. The $4d^1\Pi_1(5)$ state is labelled in Hund's case (b) notation. The asterisk indicates mixing with the $5d1_3(3)$ state.

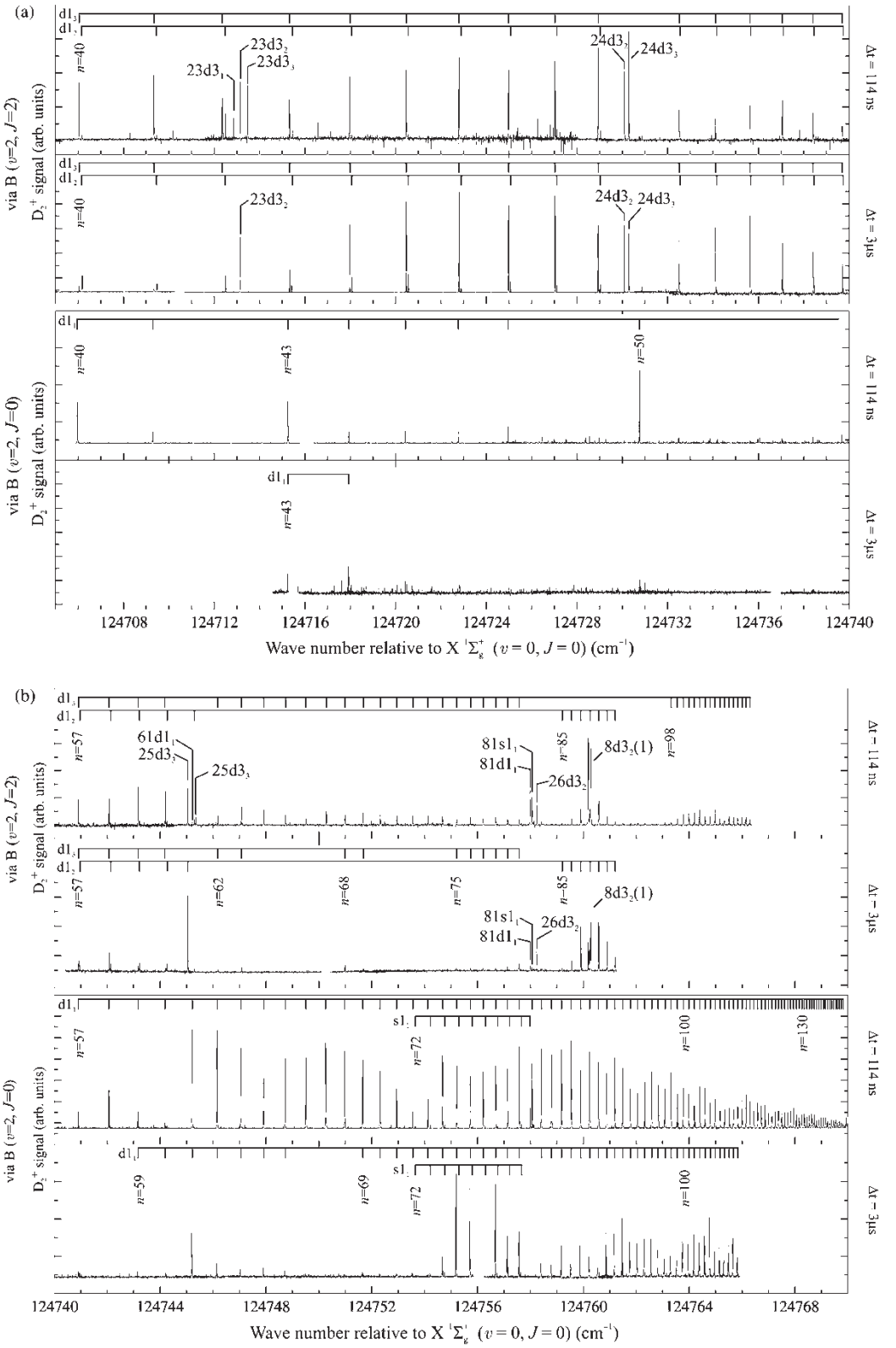

Figure 3. High-resolution pulsed field ionization spectra of D_2 obtained in the ranges (a) 124 705–124 740 cm^{-1} and (b) 124 740–124 770 cm^{-1} by scanning the UV wave number while leaving the VUV wave number tuned to either the R(1) (upper panels) or the P(1) (lower panels) lines of the $B\,^1\Sigma_u^+$ $(v = 2) \leftarrow X^1\Sigma_g^+$ $(v = 0)$ transition. In each panel, the upper and lower traces correspond to spectra measured at a delay between excitation and pulsed field ionization of 114 ns and 3 μs, respectively. The wave number scale is relative to the position of the $X\,^1\Sigma_g^+$ $(v = 0, J = 0)$ ground neutral state of D_2.

form D($n=2$) on a timescale of less than 10 ns. The ions were extracted 160 ns after the laser pulse using a pulsed extraction electric field of 400 V/cm. All signals observed in panels (a) and (c) below the first ionization threshold ($N^+=1$) therefore correspond to D_2^+ ions produced by the electric field ionization of long-lived Rydberg states.

The spectra recorded in the D_2^+ mass channel reveal extended d Rydberg series converging on the $N^+=1$ and $N^+=3$ thresholds (panels (a) and (c)). The full width at half maximum of the narrowest resonances amounts to 0.15 cm^{-1}, limited by the UV laser bandwidth, which is insufficient to resolve the individual N fine-structure components.

The other features observed in figure 2 are transitions to low-n Rydberg states belonging to series converging on vibrationally excited levels of the D_2^+ ion. As anticipated on the basis of the smaller vibrational constant of D_2^+, the density of interlopers in the spectrum of D_2 is higher than in the corresponding region of the spectrum of H_2 [15]. They were assigned on the basis of multichannel-quantum-defect-theory calculations using preliminary quantum defect curves which were calculated *ab initio* [49]. The positions and assignments of these vibrational interlopers are listed in table 2.

Table 2. Principal vibrational interlopers in the photoionization spectrum of D_2 in the vicinity of the $D_2^+(v^+=0)$ ionization threshold. Owing to the widths of the resonances and the slight nonlinearity of the experimental scans, the spectral positions are only quoted to a precision of 1 cm^{-1}.

$\tilde{\nu}$ *wrt* $X\,^1\Sigma_g^+(v=0,\ J=0)(cm^{-1})$	Assignment nlN_N^+ (v^+)
124 606	$8d1_1(1)$
124 735	$8d3_1(1)$
124 754	$6d1_1(2)$
124 761	$8d3_2(1)$
124 763	$8d3_3(1)$
124 805	$6d1_2(2)$
124 817	$5d1_1(3)$
124 858	$4d1_1(5)$[a]
124 872	$5d1_2(3)$
124 879	$5d1_3(3)$
124 899	$6d3_1(2)$[b]
124 905	$4d3_2(5)$[c]
124 921	$6s1_1(2)$
124 927	$6d3_2(2)$
124 931	$6d3_3(2)$
124 976	$9d1_1(1)$

[a]This state is better described in case (b) notation as 4d $^1\Pi_g^+(v=5, N=1)$.
[b]This state is very strongly mixed with the $5d3_1$ (3) state.
[c]This state is better described in case (b) notation as 4d $^1\Pi_g^-(v=5, N=2)$.

The transitions to the low-n interlopers are the most intense features in the spectra because the Franck–Condon factors are appreciable and the intensities of transitions to Rydberg states scale as $1/n^3$. The larger widths of the transitions to the low-n interlopers compared with those of the transitions to the high-n, $v^+=0$ Rydberg states reflect faster decay dynamics by predissociation, autoionization, or both. In several cases, satellite lines are visible on each side of the interloper lines. These satellite lines, which are part of high-n Rydberg series converging to either the $v^+=0$, $N^+=1$ or 3 thresholds, gain intensity as a result of vibrational channel interactions. The line clusters around the interlopers are typical features of the Rydberg spectrum of molecular hydrogen and are usually referred to as complex resonances [5]. The broadest complex resonances are those associated with $v^+=1$ interlopers ($8d1_1(1)$, $8s1_1(1)$, $8d3_1(1)$ and $8d3_3(1)$), an observation that can be explained by the fact that vibrational channel interactions are strongest for the smallest values of $|\Delta v|$ [2].

Below the $N^+=1$ threshold the interlopers appear almost exclusively in the dissociation channel (panels (b) and (d)). Predissociation is induced in this region by the $(2p\sigma_u)^2\,^1\Sigma_g^+$ repulsive state. The only interloper not to be affected by predissociation in this region is the $8d3_2(1)$ level of negative Kronig's parity index, which does not possess Σ character and therefore is not coupled to the repulsive state. This state appears in the D_2^+ channel in panel (a) and is observed as a result of forced vibrational autoionization when the electric field pulse is applied.

The effects of the predissociative interlopers are also noticeable in the D_2^+ channel. The intensities of the nd1 and nd3 series are strongly suppressed around the positions of the $8d1_1(1)$, $8s1_1(1)$, $8d3_1(1)$ and $6d1_1(2)$ resonances because the vibrational channel interactions induce the predissociation of the $v^+=0$ high-n Rydberg levels involved in the complex resonances. However, it is only in the immediate vicinity of the centre of the complex resonances that the predissociation is fast enough for the signal to be detected in the D^+ mass channel.

3.2. *High-resolution spectra of D_2 below the $v^+=0$, $N^+=1$ threshold recorded via the $B\,^1\Sigma_u^+$ ($v'=2, J'=0$, and 2) intermediate levels*

The high-resolution pulsed field ionization spectra of D_2 displayed in figures 3(a) and (b) were obtained by scanning the UV wave number while leaving the VUV wave number tuned to either the R(1)

(upper panels) or the P(1) (lower panels) lines of the $B\,^1\Sigma_u^+$ ($v' = 2$) $\leftarrow$ $X\,^1\Sigma_g^+$ ($v = 0$) transition. In each panel, the upper and lower traces correspond to spectra measured at a delay between excitation and pulsed field ionization of 114 ns and 3 µs, respectively. The narrowest lines in these spectra have a full width at half maximum of about 300 MHz, which is sufficient to resolve the N fine structure up to $n \approx 60$. A comparison of the signal intensities for the two different delay times enables one to identify all long-lived states. The perturbations in line positions, intensities and lifetimes caused by the low-v^+ interlopers discussed in the previous subsection are also visible in the high-resolution spectra of figure 3. The ability to resolve and assign the N fine structure of the $v^+ = 0$ series enables one to determine the N quantum numbers of the interlopers and to confirm the assignments presented in table 2. For example, the nd1$_2$ series gains intensity at $\approx 124\,760\,\mathrm{cm}^{-1}$ in the spectra recorded via the $J' = 2$ intermediate level (see figure 3(b)). The interloper must therefore be an $N = 2$ level (8d3$_2$(1)).

In the spectra recorded via the $J' = 2$ intermediate level, the most prominent of the series converging to $N^+ = 1$ is the nd1$_3$ series. This series carries intensity over most of the wave number range scanned. The nd1$_2$ series is identified as a less intense series of peaks to the higher energy side of the nd1$_3$ lines, and neither the ns1$_1$ nor the nd1$_1$ series are observed. Perturbations of the series intensities and positions caused by interloper states converging on higher rotational and vibrational levels of the ion are clearly observed in these spectra. Next to the complex resonance with an overall width of $\approx 2\,\mathrm{cm}^{-1}$ associated with the 8d3$_2$(1) interloper mentioned above, the sudden increase of the intensity of the nd1$_3$ series beyond $124\,764\,\mathrm{cm}^{-1}$ can be attributed to a perturbation caused by the 8d3$_3$(1) interloper. The 8d3$_3$(1) interloper, however, is not observed in the delayed pulsed field ionization spectra because it is predissociative as discussed in subsection 3.1. Local perturbations caused by rotational channel interactions also represent prominent features of the spectra. Examples are the regions around the transitions to the 23–26d3$_N$ ($N = 1 - 3$) levels.

Spectra recorded via the $J' = 0$ intermediate state are dominated by the nd1$_1$ series which is observed between $n = 40$ ($124\,706.0\,\mathrm{cm}^{-1}$) and $n = 165$ ($124\,770.5\,\mathrm{cm}^{-1}$). The series undergoes strong intensity fluctuations below $124\,745\,\mathrm{cm}^{-1}$ caused by the $N = 1$ interlopers listed in table 2 but becomes regular beyond $n \approx 75$. The s1$_1$ series is only identified as a series of weak lines located on the higher wave number side of the d1$_1$ lines in the range $n = 72 - 80$ ($124\,753.5$–$124\,757.5\,\mathrm{cm}^{-1}$).

The lifetimes of the nd1$_3$ and nd1$_2$ Rydberg states exceed 0.5 µs from $n = 38$ ($124\,699.0\,\mathrm{cm}^{-1}$) to $n = 60$ ($124\,744.0\,\mathrm{cm}^{-1}$). We conclude that the lifetimes of the nd1$_3$ Rydberg states are shorter than those of the nd1$_2$ Rydberg states because the relative intensities between the two series change in favour of the nd1$_2$ series at longer delay times; whereas the nd1$_3$ Rydberg states have lifetimes of ≈ 1 µs, the nd1$_2$ Rydberg levels do not decay significantly on the experimental time scale of 3 µs. This metastability can be explained by the fact that they have no Σ character and therefore cannot couple to the repulsive $(2p\sigma_u)^2\,^1\Sigma_g^+$ state. The observed s1$_1$ states are long-lived ($\tau \geq 1$ µs), but they only carry intensity over a narrow range of n values between 72 and 80. The members of the nd1$_1$ series are long-lived beyond $n = 74$. Below $n = 74$, only isolated members of this series located in the immediate vicinity of nd3$_1$ rotational interlopers are long-lived (e.g. 43d1$_1$, 44d1$_1$, 50d1$_1$ and 61d1$_1$). Several of the Rydberg states belonging to series converging on the $N^+ = 3$ rotational levels, and which perturb the $N^+ = 1$ series, are also long-lived, such as the 23d3$_2$, 24d3$_{2,3}$, 25d3$_{2,3}$ and 26d3$_2$ states. A list of all observed Rydberg states with lifetimes longer than ≈ 1 µs is presented in table 3.

3.3. *MQDT analysis, assignment of rotational interlopers, and ionization energies*

In order to model the perturbations caused by interactions with channels associated with higher rotational levels of the D_2^+ ion and to conclusively assign these rotational interlopers, the spectra were analysed using an MQDT model describing all series converging on the $v^+ = 0$ threshold, in which a frame transformation

Table 3. Observed s and d Rydberg states of D_2 with lifetimes longer than ≈ 1 µs.

Excitation scheme	Observed series	Long-lived states ($\tau \geq 1$ µs)	Long-lived interlopers
Via R(1)	nd1$_2$	$n = 38$–50, 52–60, 85–91	23d3$_2$, 24d3$_{2,3}$
	nd1$_3$	$n = 40$–49, 51–60	25d3$_{2,3}$, 26d3$_2$
			8d3$_2$(1)
Via P(1)	ns1$_1$	$n = 72$–80	
	nd1$_1$	$n = 43$, 44, 50, 61, 74–111+	

from Hund's case (b) to Hund's case (d) was performed. A calculation neglecting the effect of spins was sufficient because the hyperfine structure of the D_2 Rydberg states was not resolved. Indeed, the largest hyperfine splittings in the high Rydberg states of para D_2 and in the lowest rotational levels of the D_2^+ ion amount to approximately 200 MHz [35], i.e. less than the 300 MHz resolution of the experiment.

The relevant channels in the Hund's case (b) and (d) representations are listed in table 4. The $\langle N^+|\lambda\rangle^{(l,N)}$ frame transformation between case (b) and case (d) channels was performed using equation (4) of [50]. The bound levels of the system were determined in a standard MQDT procedure using η quantum defects [51] by solving

$$\det\left|\frac{\tan\pi\nu_i(E)\delta_{i,i'}}{A(E,l_i)}+\tan\pi\eta_{i,i'}\right|=0, \qquad (2)$$

where

$$\nu_i(E)=\left[\frac{\mathrm{Ry}_M}{E_i^+-E}\right]^{1/2}. \qquad (3)$$

In equations (2) and (3) E represents the total energy, ν is the effective principal quantum number, the subscript i denotes the Rydberg channel and the associated state of the ion core of energy E_i^+ and $\delta_{i,i'}$ stands for Kronecker's delta. A is Ham's scaling function, which is given by equation (2.31) of [52] and Ry_M is the mass-corrected Rydberg constant, which takes a value of 109 722.27 cm^{-1} for D_2.

R-independent η quantum defects (R is the internuclear distance) and the ionization limits from the selected intermediate levels were fitted to the observed positions of the transitions from the B $v=2$, $J=0$ level to the $n=40$, 41, 43–47, 50, 56–80, and 86–126 $\mathrm{d1}_1$ and the $n=72-80$ $\mathrm{s1}_1$ Rydberg states, and from the B $v=2$, $J=2$ level to the $n=38-46$, 48, 49 and 51–61 $\mathrm{d1}_2$ and the $n=38-49$, 51–60 and 62–80 $\mathrm{d1}_3$ Rydberg states. In addition, the positions of the $23\mathrm{d3}_1$, $23\mathrm{d3}_2$, $23\mathrm{d3}_3$, $24\mathrm{d3}_2$, $24\mathrm{d3}_3$, $25\mathrm{d3}_2$ and $25\mathrm{d3}_3$ were also used in the MQDT fit. Inspection of the spectra presented in figures 2 and 3 reveals that the corresponding spectral regions are largely unaffected by perturbing states belonging to series converging on higher vibrational thresholds. Therefore, the calculations only included channels associated with the $v^+=0$ threshold. The resulting effective case (b) η quantum defects for the $v^+=0$ channels are listed in table 5 and were determined in a simultaneous fit to the transitions recorded via the $J=0$ and 2 intermediate levels. To place both sets of transitions on the same wave number scale, the spectrum recorded via the $J=2$ intermediate level was shifted with respect to the spectrum recorded via the $J=0$ level until the positions of the $81\mathrm{d1}_1$ level, which was observed in both spectra, coincided.

The MQDT calculation reproduces the experimental line positions with an average error of less than 0.007 cm^{-1}, which is smaller than the full width at half maximum of most transitions and only slightly larger than the uncertainty in the determination of the relative line positions (see table 1). Model calculations of the intensity distributions based on the p $\rightarrow$ *gerade* transition moments determined by Texier and Jungen [53] also broadly reproduce the experimentally observed intensity patterns. In particular, the $\mathrm{s1}_1$ series is predicted to be very weak when populated via either the $J=0$ or 2 rotational levels of the intermediate state, owing to low transition moments. The reason for the complete absence of the $n\mathrm{d1}_1$ series in the spectra recorded from the $J=2$ level of the B state lies in a destructive interference effect.

In the region over which the fit was performed, rotational perturbers with $n=23$ to $n=25$ associated

Table 5. Effective case (b) η quantum defects for the $v^+=0$ ionization channels of D_2 determined from a fit to the experimental data. The last row lists the off-diagonal quantum defect describing the interaction between s and d channels of Σ_g^+ symmetry.

$\mathrm{s}\,^1\Sigma_g^+$	−0.0990(30)
$\mathrm{d}\,^1\Sigma_g^+$	0.0827(10)
$\mathrm{d}\,^1\Pi_g$	0.0450(5)
$\mathrm{d}\,^1\Delta_g$	−0.0132(20)
$\mathrm{sd}\,^1\Sigma_g^+$	0.0157(60)

Table 4. Ionization channels in the Hund's case (b) and (d) representations accessible from the ground neutral state of D_2 following resonant two-photon excitation via the $J=0$ and 2 rotational levels of the $\mathrm{B}\,^1\Sigma_u^+$ state. Only the $N=1$ channels are accessible via the $J=0$ intermediate level.

N	Case (b) channels				Case (d) channels				
1	$ns\,^1\Sigma_g^+$	$n\mathrm{d}\,^1\Sigma_g^+$	$n\mathrm{d}\,^1\Pi_g^+$		$ns1_1$	$n\mathrm{d}1_1$		$n\mathrm{d}3_1$	
2			$n\mathrm{d}\,^1\Pi_g^-$	$n\mathrm{d}\,^1\Delta_g^-$		$n\mathrm{d}1_2$		$n\mathrm{d}3_2$	
3	$ns\,^1\Sigma_g^+$	$n\mathrm{d}\,^1\Sigma_g^+$	$n\mathrm{d}\,^1\Pi_g^+$	$n\mathrm{d}\,^1\Delta_g^+$		$n\mathrm{d}1_3$	$ns3_3$	$n\mathrm{d}3_3$	$n\mathrm{d}5_3$

with the $v^+ = 0$, $N^+ = 3$ threshold are observed. The regions around the $n = 23$ and 24 perturbers are displayed on an enlarged scale in figures 4(a) and (b), respectively. In these figures, the upper and middle traces correspond to spectra recorded via the B($v = 2$) $J = 2$ and $J = 0$ intermediate levels, respectively. The lowest trace of each panel represent stick spectra indicating the positions calculated by MQDT where the full, dashed and dotted lines represent levels with $N = 1$, 2 and 3, respectively. Only calculated lines that have not been observed and assigned in the top two traces are labelled in these spectra. At each principal quantum number, four states are expected, corresponding to members of the $d3_1$, $d3_2$, $d3_3$ and $s3_3$ series. However, the $s3_3$ series is never observed and the $d3_1$ series is only detected at $n = 23$ because the $24d3_1$ and $25d3_1$ states couple to the vibrationally excited $8d3_1$ ($v^+ = 1$) state and predissociate rapidly (see figure 2). The $d3_2$ and $d3_3$ series are observed in each case, although the $25d3_3$ line is weak. The observed and calculated positions of the rotational interlopers with respect to the $B\,^1\Sigma_u^+$ ($v = 2$, $J = 2$) level are listed in table 6.

The large number of Rydberg levels measured from $n = 40$ to beyond $n = 100$ enables the accurate determination of the energy separation between the $X^+2\Sigma_g^+$ ($v^+ = 0, N^+ = 1$) ionic level and the $B\,^1\Sigma_u^+$ ($v = 2, J = 0$ and 2) intermediate levels using an extrapolation based on separate MQDT fits of the transitions recorded from the $J = 0$ and $J = 2$ intermediate levels. We find the $X^+(v^+ = 0, N^+ = 1) - B^+(v = 2, J = 0)$ interval to be $32\,276.110 \pm (0.009)^{1\sigma}_{\text{stat}} \pm (0.011)_{\text{sys}}\,\text{cm}^{-1}$ and the $X^+(v^+ = 0, N^+ = 1)$–$B(v = 2, J = 2)$ interval to be $32\,221.096 \pm (0.009)^{1\sigma}_{\text{stat}} \pm (0.011)_{\text{sys}}\,\text{cm}^{-1}$. The statistical error in the MQDT fit of the ionization energy slightly exceeds the relative uncertainty expected for each line position (see upper part of table 1), probably because the MQDT model does not include $v^+ \geq 1$ ionization channels. From the known interval of $29.3910\,\text{cm}^{-1}$ between the $N^+ = 0$ and 1 rotational levels of the $X^+\,^2\Sigma_g^+(v^+ = 0)$ state of D_2^+ [54, 55] and the latest experimental value of $124\,745.362(24)\,\text{cm}^{-1}$ [32, 56] or the latest theoretical value of $124\,745.395\,\text{cm}^{-1}$ [57] for the adiabatic ionization energy of D_2, the absolute position of the $B(v = 2, J = 0)$ level can be inferred to be $92\,498.643(28)\,\text{cm}^{-1}$ or $92\,498.676\,\text{cm}^{-1}$, respectively. These values lie close to, but outside the error margins of Wilkinson's result of $92\,498.80 \pm 0.054\,\text{cm}^{-1}$ [58]. A new measurement of the B–X(2–0) Lyman band of D_2 would enable one, with the help of the present result for the X^+–B intervals, to determine whether the current discrepancy between theory and experiment concerning the adiabatic ionization energy of D_2 has an experimental origin.

4. Conclusions

The present investigation of the high-n gerade Rydberg states of para D_2 in the vicinity of the adiabatic ionization threshold has revealed the complex structure and dynamics of these levels. The resolution of 300 MHz achieved in the present experiments was insufficient to observe the hyperfine structure of the Rydberg levels and the largest hyperfine splittings must be less than 250 MHz, i.e. more than six times less than in H_2, as expected from the different magnetogyric ratios of the proton and the deuteron.

Predissociation mediated by the low-n Rydberg levels associated with vibrationally excited core levels is the main source of decay of the high-n Rydberg levels converging to the lowest level of para D_2^+ ($N^+ = 1$). The higher density of these interlopers compared with H_2, which results from the smaller vibrational and rotational constants of the ion core, reduces the number of truly long-lived Rydberg states. Nevertheless, numerous Rydberg states are long-lived.

The main metastable series is the $nd1_2$ series which, by virtue of its symmetry, is not coupled to the repulsive $(2p\sigma_u^+)^2\,^1\Sigma_g^+$ doubly excited state. Unfortunately, this series is weak. Two series that are suitable for millimeter wave spectroscopic experiments to measure the hyperfine structure in gerade and ungerade Rydberg states of D_2 are the $nd1_1$ series beyond $n = 74$ and the $nd1_3$ series between $n = 40$ and 60. The strength of the $nd1_3$ series and the convenient range of n values of the long-lived levels make these levels particularly attractive for such measurements. From the lifetimes of ≈ 0.5–1 μs of these levels, a resolution of about 1 MHz can be achieved by millimeter wave spectroscopy. Measurements are underway in our laboratory in which we observe the hyperfine structure of Rydberg–Rydberg transitions to determine, by extrapolation, the hyperfine structure of the D_2^+ cation [35].

Recently, a new method has been established to control the velocity distributions of Rydberg atoms and molecules based on the Stark effect and the large forces that can be applied on Rydberg atoms and molecules using inhomogeneous electric fields [36, 37, 59, 60]. The time scale of these experiments lies in the microsecond range and can only be applied to molecular systems with sufficiently long-lived Rydberg Stark states. The method has been successfully applied to decelerate and deflect beams of H_2 Rydberg molecules [36, 37]. From a comparison of the lifetimes and decay mechanisms of the Rydberg levels of D_2 observed in the present investigation with those observed in H_2 in similar experiments [15], we expect that D_2 represents another molecular system that is well suited to these experiments.

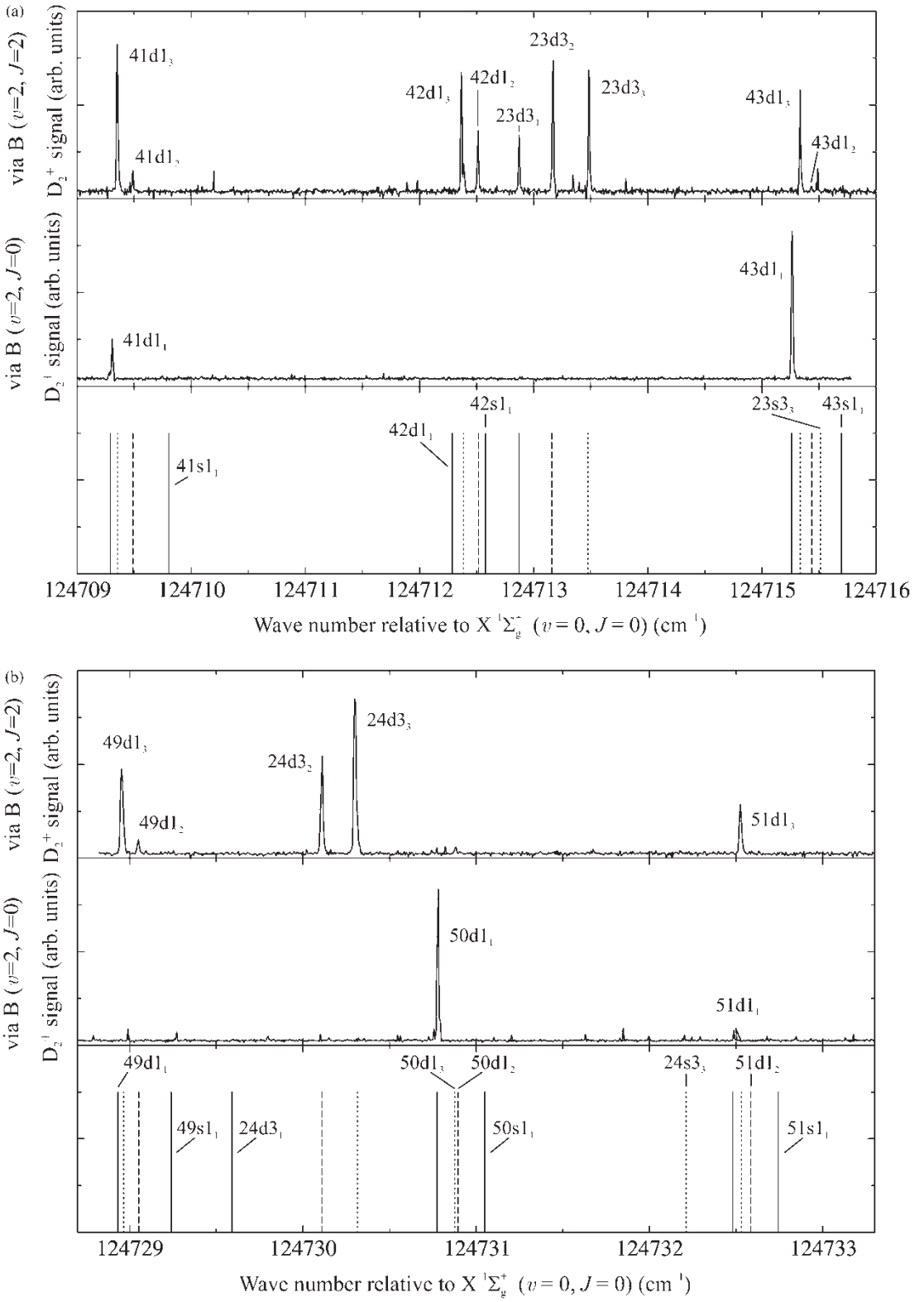

Figure 4. Enlarged view of the regions of the pulsed-field-ionization spectra of D_2 around the $n=23$ (a) and 24 (b) rotational perturbers. In each panel, the upper and middle traces correspond to spectra recorded via the B ($v=2$) $J=2$ and $J=0$ intermediate levels, respectively. The lowest trace shows stick spectra indicating the positions calculated by MQDT where the full, dashed and dotted lines represent levels with $N=1$, 2 and 3, respectively. The wave number scale is relative to the position of the $X\,^1\Sigma_g^+$ ($v=0, J=0$) ground neutral state of D_2.

Table 6. Positions, relative to the $B^1\Sigma_u^+(v = 2, J = 2)$ level, of the observed $nd3_N(v^+ = 0)$ rotational interlopers below the $v^+ = 0, N^+ = 1$ ionization threshold of para D_2.

State (nlN_N^+)	$\tilde{\nu}_{obs}$ wrt $B\ ^1\Sigma_u^+(v = 2,\ J = 2)$ (cm^{-1})	$\tilde{\nu}_{obs} - \tilde{\nu}_{calc}$ (cm^{-1})
$23d3_1$	32 159.189	−0.001
$23d3_2$	32 159.487	0.010
$23d3_3$	32 159.802	0.010
$24d3_2$	32 176.427	0.001
$24d3_3$	32 176.618	−0.013
$25d3_2$	32 191.381	−0.014
$25d3_3$	32 191.689	−0.009

Acknowledgements

We thank Dr. Ch. Jungen (Orsay) for useful discussions and for making several MQDT routines available to us. This work is supported financially by the Swiss National Science Foundation under project 200020-108080 and the ETH Zurich.

References

[1] U. Fano, Phys. Rev. A **2,** 353 (1970); see erratum in [61].
[2] G. Herzberg and Ch. Jungen, J. Molec. Spectrosc. **41,** 425 (1972).
[3] P. M. Dehmer and W. A. Chupka, J. Chem. Phys. **65,** 2243 (1976).
[4] Ch. Jungen and O. Atabek, J. Chem. Phys. **66,** 5584 (1977).
[5] M. Raoult and C. Jungen, Faraday Discuss. **71,** 253 (1981).
[6] S. T. Pratt, P. M. Dehmer, and J. L. Dehmer, Chem. Phys. Lett. **105,** 28 (1984).
[7] S. T. Pratt, P. M. Dehmer, and J. L. Dehmer, J. Chem. Phys. **86,** 1727 (1987).
[8] S. Ross and Ch. Jungen, Phys. Rev. Lett. **59,** 1297 (1987).
[9] H. Rottke and K. H. Welge, J. Chem. Phys. **97,** 908 (1992).
[10] S. C. Ross and Ch. Jungen, Phys. Rev. A **49,** 4353 (1994).
[11] S. C. Ross and Ch. Jungen, Phys. Rev. A **49,** 4364 (1994).
[12] S. C. Ross and Ch. Jungen, Phys. Rev. A **50,** 4618 (1994).
[13] W. L. Glab, K. Qin, and M. Bistransin, J. Chem. Phys. **102,** 2338 (1995).
[14] C. R. Scheper, W. J. Buma, C. A. de Lange, and W. J. van der Zande, J. Chem. Phys. **109,** 8319 (1998).
[15] A. Osterwalder, A. Wüest, F. Merkt, and Ch. Jungen, J. Chem. Phys. **121,** 11810 (2004).
[16] L. Wolniewicz and K. Dressler, J. Chem. Phys. **100,** 444 (1994).
[17] A. Osterwalder, R. Seiler, and F. Merkt, J. Chem. Phys. **113,** 7939 (2000).
[18] O. Atabek, D. Dill, and Ch. Jungen, Phys. Rev. Lett. **33,** 123 (1974).
[19] S. Bezzaouia, M. Telmini, and Ch. Jungen, Phys. Rev. A **70,** 012713 (2004).
[20] S. Takezawa and Y. Tanaka, J. Chem. Phys. **56,** 6125 (1972).
[21] P. M. Dehmer and W. A. Chupka, J. Chem. Phys. **79,** 1569 (1983).
[22] G. M. Greetham, U. Hollenstein, R. Seiler, W. Ubachs, and F. Merkt, Phys. Chem. Chem. Phys. **5,** 2528 (2003).
[23] N. Y. Du and C. H. Greene, J. Chem. Phys. **85,** 5430 (1986).
[24] F. Merkt, H. Xu, and R. N. Zare, J. Chem. Phys. **104,** 950 (1996).
[25] H. Bedrohl and G. Herzberg, Can. J. Phys. **51,** 867 (1973).
[26] I. Dabrowski and G. Herzberg, Can. J. Phys. **52,** 1110 (1974).
[27] P. Borrell, P. M. Guyon, and M. Glass-Maujean, J. Chem. Phys. **66,** 818 (1977).
[28] W. A. Chupka, P. M. Dehmer, and W. T. Jivery, J. Chem. Phys. **63,** 3929 (1975).
[29] P. Senn, P. Quadrelli, K. Dressler, and G. Herzberg, J. Chem. Phys. **85,** 2384 (1986).
[30] P. Senn and K. Dressler, J. Chem. Phys. **87,** 6908 (1987).
[31] S. T. Pratt, P. M. Dehmer, and J. L. Dehmer, Chem. Phys. Lett. **165,** 131 (1990).
[32] Ch. Jungen, I. Dabrowski, G. Herzberg, and M. Vervloet, J. Molec. Spectrosc. **152,** 11 (1992).
[33] J. M. Gilligan and E. E. Eyler, Phys. Rev. A **46,** 3676 (1992).
[34] R. S. Freund, J. A. Schiavone, and H. M. Crosswhite, J. Phys. Chem. Ref. Data **14,** 235 (1985).
[35] H. A. Cruse, Ch. Jungen, and F. Merkt, to be published.
[36] S. R. Procter, Y. Yamakita, F. Merkt, and T. P. Softley, Chem. Phys. Lett. **374,** 667 (2003).
[37] Y. Yamakita, S. R. Procter, A. L. Goodgame, T. P. Softley, and F. Merkt, J. Chem. Phys. **121,** 1419 (2004).
[38] T. P. Softley, Int. Rev. Phys. Chem. **23,** 1 (2004).
[39] F. Aguirre and S. T. Pratt, J. Chem. Phys. **121,** 9855 (2004).
[40] P. Rupper and F. Merkt, Rev. Sci. Instrum. **75,** 613 (2004).
[41] Th. A. Paul and F. Merkt, J. Phys. B **38,** 4145 (2005).
[42] R. Seiler, Th. A. Paul, M. Andrist, and F. Merkt, Rev. Sci. Instrum. **76,** 103103 (2005).
[43] U. Hollenstein, H. Palm, and F. Merkt, Rev. Sci. Instrum. **71,** 4023 (2000).
[44] H. Katô, M. Baba, S. Kasahara, K. Jshikawa, M. Misono, Y. Kimura, J. O'Reilly, H. Kuwano, T. Shimamoto, T. Shianano, C. Fujiwara, M. Ikeuchi, N. Fujita, M. H. Kabir, M. Ushino, R. Takahashi and Y. Matsunobu, *Doppler-Free High Resolution Spectral Atlas of Iodine Molecule 15 000 to 19 000 cm^{-1}* (Japan Society for the Promotion of Science, Tokyo, 2000).

[45] S. Gerstenkorn and P. Luc, *Atlas du Spectre d'Absorption de la Molécule d'Iode—14 800–20 000 cm^{-1}* (Laboratoire Aimé-Cotton CNRS II, Orsay, 1979); see correction in [62].
[46] H. Knöckel, B. Bodermann, and E. Tiemann, Eur. Phys. J. D **28,** 199 (2004). The reference data for calibration were derived from a calculation of the iodine hyperfine structure by the IodineSpec program.
[47] U. Hollenstein, R. Seiler, and F. Merkt, J. Phys. B **36,** 893 (2003).
[48] The line tables of the appendix have been deposited with the British Library Document Supply Center: The reference number is SUP 16177 (for further information, please consult the second page of 'submitting a paper' of *Molecular Physics*).
[49] H. J. Wörner, M. Telmini, H. Oueslati, and Ch. Jungen, to be published.
[50] K. P. Huber, Ch. Jungen, K. Yoshino, K. Ito, and G. Stark, J. Chem. Phys. **100,** 7957 (1994).
[51] Ch. Jungen (Editor), *Molecular Applications of Quantum Defect Theory* (Institute of Physics Publishing, Bristol, 1996).
[52] M. J. Seaton, Rep. Prog. Phys. **46,** 167 (1983).
[53] F. Texier and Ch. Jungen, Phys. Rev. Lett. **81,** 4329 (1998).
[54] R. E. Moss, Chem. Phys. Lett. **206,** 83 (1993).
[55] R. E. Moss, J. Phys. B **32,** L89 (1999).
[56] A. Yiannopoulou, N. Melikechi, S. Gangopadhyay, J. C. Meiners, C. H. Cheng and E. E. Eyler, Phys. Rev. A **73,** 022506 (2006).
[57] L. Wolniewicz, J. Chem. Phys. **103,** 1792 (1995).
[58] P. G. Wilkinson, Can. J. Phys. **46,** 1225 (1968).
[59] E. Vliegen, H. J. Wörner, T. P. Softley, and F. Merkt, Phys. Rev. Lett. **92,** 033005 (2004).
[60] E. Vliegen and F. Merkt, Phys. Rev. Lett. **97,** 033002 (2006).
[61] U. Fano, Phys. Rev. A **15,** 817 (1977); see also [1].
[62] S. Gerstenkorn and P. Luc, Rev. Phys. Appliquée **14,** 791 (1979).